Nonlinear Seismic analysis of masonry bridges under multiple geometric and material considerations: application to an existing seven spans arch bridge

Abstract

Resilient infrastructure is nowadays attracting attention when designing new infrastructure projects. However, many countries around the world still have a large stock of existing transport infrastructure, such as railways and roads. In particular, masonry bridges are significantly widespread in Europe. These bridges, built a long time ago could suffer structural damage due to earthquakes, as their design in the past did not take this into account. The issue becomes critical because the scientific world still lacks cutting-edge monitoring techniques and calculation tools to accurately assess the integrity of bridges. These steps are fundamental before any maintenance activities are developed by infrastructure managers. In this study, the seismic behaviour of a seven spans masonry arch bridge is intensively investigated in order to provide new insights into the seismic vulnerability analysis of existing masonry bridges. In particular, parametric analyses are carried out to assess the effect of haunching, fill, and pier cross-section types on the seismic capacity of multi-span masonry bridges. Interesting observations were made on the change in ductility, capacity, and stiffness of the structure when the studied parameters are modified.

Keywords: Masonry Bridge, masonry, masonry arch, multi-span bridge, seismic capacity, pushover analysis, FEM, 3D model

1. Introduction

They are a tremendous amount of existing bridges around the world. Among them, masonry arch bridges are considered a cultural heritage in Italy, Europe and the rest of the world [1], which need to be preserved. Their construction dates back mainly between the end of the nineteenth century and the beginning of the twentieth century [2], a period characterized by the important development of communication networks, road and railway systems in many countries of the world. However, the increase in traffic loads and the recent occurrence of seismic actions [3], combined with the effects of material degradation [4-5], have recently led to a more in-depth study of the structural behaviour of these bridges throughout the use of different modelling techniques [6–12]. For instance, many scientists in civil engineering are now looking for effective methods of analysis, and the assessment of the structural safety of these types of bridges. Also, they currently focus their studies on the static and dynamic behaviour of structures that have been built on the basis of simple notions of equilibrium [13]. Even though characterized with complex mechanical behaviour, significant progress has been observed thanks to numerous studies from computational mechanics [14] and experimental campaigns [15]. The analysis of the structural vulnerability of masonry bridges in a more sophisticated calculation can be done either by a detailed three-

dimensional finite element [16-21] or discrete element models [10, 21–24]. However, such analysis strategies require a high computational effort and are difficult to be used in common engineering practice. For these reasons, over the years, some researchers have focused their research on the development of simple and reliable methods that could provide results quickly and easily be interpreted by bridge engineers. With this objective in mind, the methods based on the limit and/or rigid-block analysis were born [6, 14, 24–33], followed by the macro-block based models [34–36] and the analysis method where the limit analysis is coupled with nonlinear analysis [37].

Another interesting line of research is the study of the behaviour of masonry bridges subjected to certain external actions that may compromise their stability. In particular, the analysis of recent collapses has shown that masonry bridges are particularly vulnerable to the phenomena that cause the failure of their supports [17, 26, 29, 38-46] and to high intensity seismic actions [47-57], as evidenced by the collapse of the Claro Bridge [58] during the 2010 Maule, Chile earthquake. In recent years, numerous studies have been developed to investigate the structural implications of foundation settlement on the bearing capacity of the bridge. Other studies have focused on the seismic behaviour of masonry bridges by defining calculation methods adapted to the type of structure examined, or on the classification of the structures in terms of seismic vulnerability.

The seismic assessment of a masonry bridge can be carried out using different analysis methods according to the recommendations collected in the national standards and international guidelines. However, non-linear analysis methods are more accurate than the linear methods in describing the seismic behaviour of masonry structures. In particular, non-linear dynamic analysis is the most widely used analysis method for the seismic assessment of masonry bridges, although the computational effort is greater than other commonly used computational strategies. For this is the reason, non-linear static (pushover) analysis represents the best balance between accuracy and computer effort and is the analysis method generally used by structural engineers for the seismic evaluation of existing masonry structures. With the aim to provide practical results useful to engineers, this paper presents the results of the pushover analysis.

In particular, in this paper, some aspects not yet explored by previous research with reference to the seismic behaviour of slender masonry bridges was analysed. In particular, the contribution of filling, haunching and spandrel walls in the overall seismic behaviour of the bridge was highlighted, with more emphasis on how these parameters (if considered as resisting elements) contribute to the definition of the bridge's strength, stiffness and dissipative capacity. Finally, the seismic behaviour of masonry bridges with hollow piers is analysed and the influence of the cross-section configuration of the piers in defining the seismic performance of the bridge will be discussed later.

2. The case study: 7-spans slender masonry arch bridge

The bridge typology investigated in this research is made of seven masonry arch spans. As shown in Figure 1, the bridge consists of almost semi-circular arches with a rise of 6.1 m and a span of 12.5 m. The vaults have a constant thickness of 1.0 m. The piers, also made of masonry, have a variable height of 18.1, 15.0 and 9.6 m (Figure 1); they are important in transferring the loads to the ground through shallow foundations of 6.5 m wide, 5.0 m deep and 3.0 m thick. The masonry abutments are 7.5 m high. At both ends of the bridge, there are haunching for a variable height h_r of 4.5 m, 5.8 m and 7.1 m. To complete the structure, fill element made of loose materials, with a height of 0.8 m was used starting from the extrados in keystone to the arches and, above this, a layer of ballast equal to 0.8 m; both layers were confined by the spandrel wall, 0.8 m thick. The total transverse dimension of the bridge is 5.0 m.

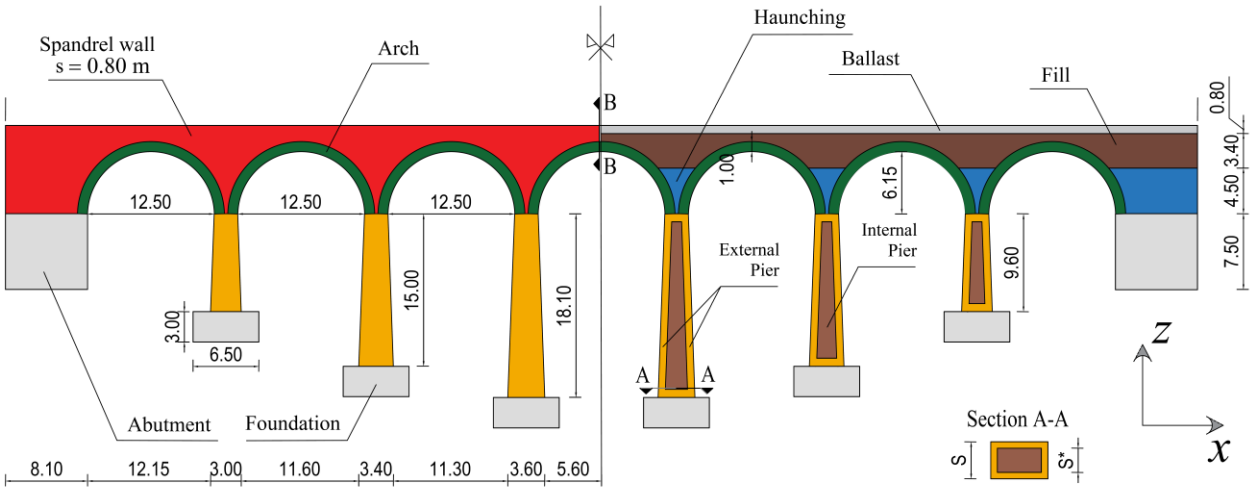

a)

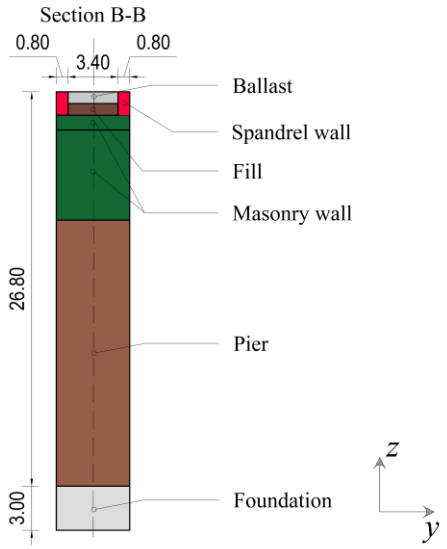

b)

Figure 1 Geometrical parameters of the masonry bridge investigated.

The bridge under investigation has slender piers and arches that make it vulnerable to seismic action. An Italian bridge with similar geometry tof the Claro River Bridge in Chile (Figure 2) was considered as the case study in this research. It is worth noting that the Claro River Bridge collapsed after an earthquake occurred off the coast of central Chile on Saturday, February 27th, 2010 with a magnitude of 8.8 on the moment magnitude scale [58].

Figure 2 Image of the Claro River Bridge before the collapse

The bridge investigated was a good example to analyse the influence of the different construction elements in the seismic response of the masonry bridge. In particular, 3D numerical models were used to assess its seismic vulnerability.

In the numerical models (Figure 3), which will be described in the next paragraph, all the structural elements of the bridge such as Pier, abutment, arches, and foundations shown in Figure 3 will be represented. Furthermore, even the non-structural elements, namely haunching, infill and spandrel walls, will be discretized using finite elements in the numerical models and not only as a dead load applied to the structure. In fact, these three elements have a fundamental role in defining the load-bearing capacity of masonry bridges even though they do not play a primary structural function. As will be illustrated below, considering them exclusively as a weight applied to the load-bearing element of the structure can lead to erroneous evaluation of the horizontal capacity and stiffness of the bridge.

In order to evaluate the influence in the seismic response of geometrical parameters of the haunching element as well as the effect of the different pier cross-sections, modal analysis and pushover analysis have been conducted considering the parameters shown in Table 1 and represented in Figure 3.

Geometry of the pier D* /D [-]	1	0.306	0.236	0.118
Haunching height h_r [m]	4.5	5.3	6.10	

Table 1 Geometric parameters of haunching and pier cross-section considered in the different analyses

Most of the time, the cross-section of the pier can be homogeneous and made of a single material. In some circumstances, masonry bridge piers are not homogeneous and consist of an outer layer made of masonry with good mechanical properties and an inner core of monolithic material with mechanical properties similar to those of the fill material.

3. Numerical models and methods of analysis

3D finite element models have been developed considering all the bridge elements (foundations, piers, arches, spandrel walls, abutments, haunching and fill as displayed in Figure 3) that contribute to its seismic resistance. These elements were discretized with solid elements (6-node pentahedron with linear shape functions and an average mesh size of 0.35 m) as presented in Figure 3.

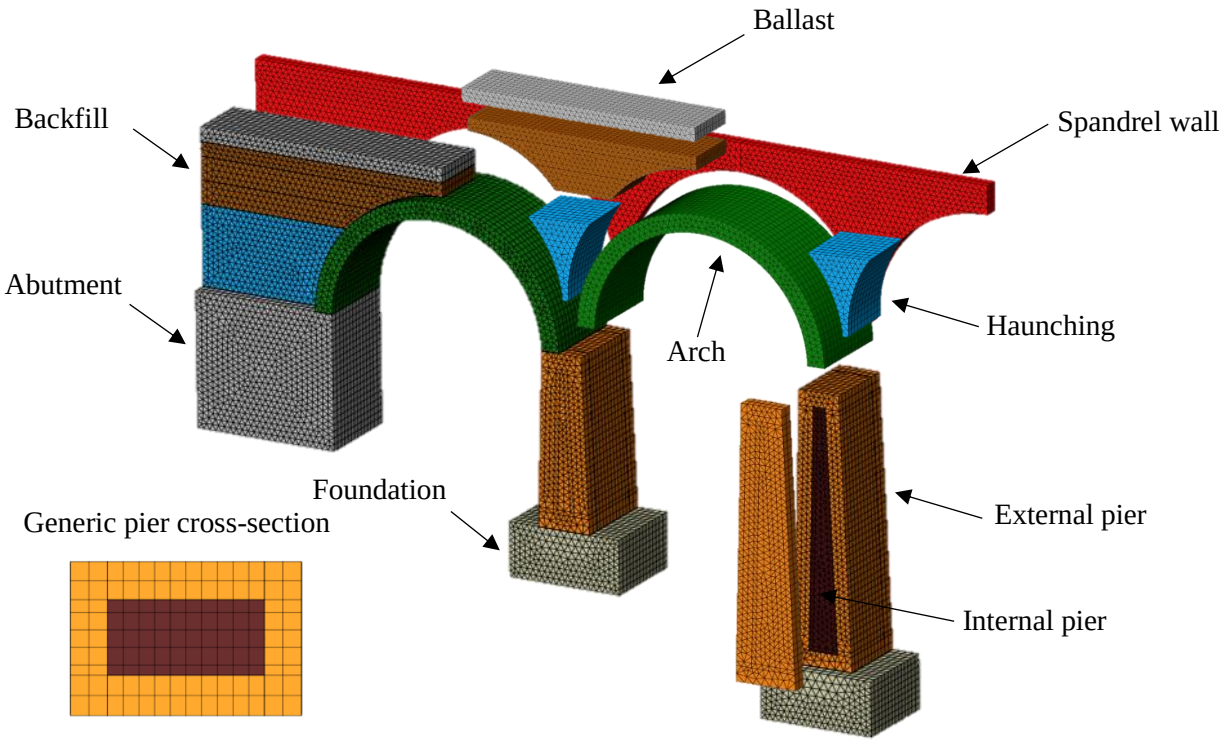

Figure 3 3D FE model detailing

The frictional contact interfaces were used to define the interaction between the infill and the arch spandrel wall using a Coulomb friction model with cohesion and dilatancy angle equal to zero. Interfaces compression normal stresses and tangential friction stresses, but zero tensile strength.

The normal stiffness k_n of the frictional contact interfaces was determined by means of a parametric analysis, where k_n was varied between the values proposed in [59] and the used value 50 N/mm^3 is the difined to optimize the numerical convergence. For increased values of k_n respect the used value the is stability of the solution. The interface tangential stiffness k_s was set equal to $0.5k_n$. The friction coefficient used si equal to 0.4 according to the scientific literature [61-62].

It is important to underline that the spandrel walls and the arch do not work perfectly in a coupled manner because the two elements have different stiffness and in addition, the spandrel walls are subjected to horizontal actions that over time tend to make the arch and spandrel walls work in a partially decoupled manner. In particular, the actions orthogonal to the plane of the spandrel walls deriving from the thrust of the infill material can be increased in intensity over time due for example, to the presence of water in these loose materials which may lead to the damage of the walls as shown in (Figure 4, (a) sliding; (b) crack opening; (c) bulging; (d) overturning. Indeed, the drainage system in masonry bridges may be malfunctioning and causes rainwater to leach through the mortar joints of the arches and also in many situations the periodic saturation of the fill material may damage the spandrel walls.

In addition, the different stiffness between the spandrel walls and the arch considering the plane parallel to the spandrel walls, in many cases causes the decoupling between them through the typical cracks as illustrated in Figure 4b. For the reasons listed above, it is appropriate to introduce a frictional contact between the arch and spandrel walls, otherwise, considering a perfect collaboration between spandrel walls and arch, the real contact behaviour between the two elements would be overestimated.

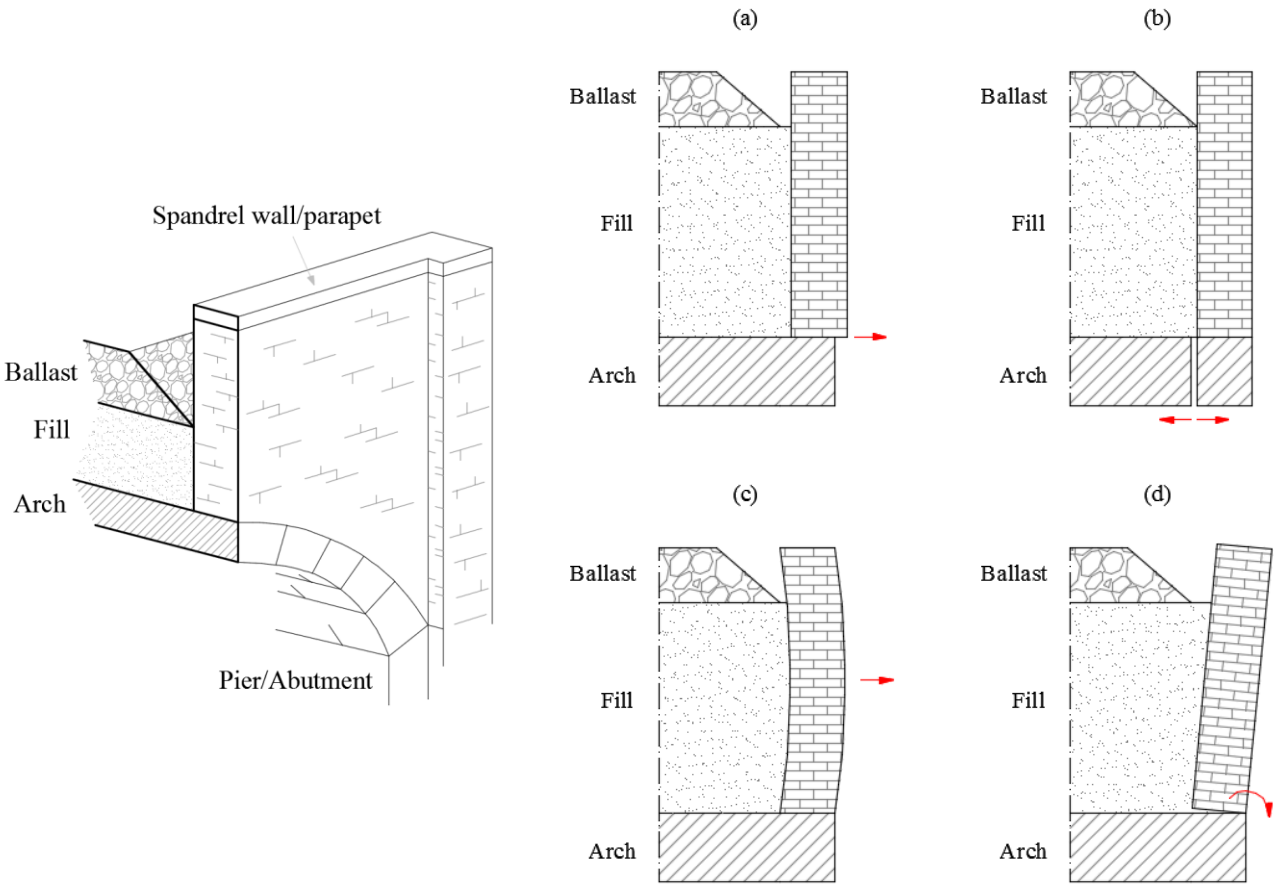

Figure 4 Axonometric section of the bridge and collapse mechanism of the spandrel wall: (a) sliding; (b) crack opening; (c) bulging; (d) overturning

The non-linearity of the material was considered by means of a continuous approach through the constitutive model called "Total Strain Crack Model (TSCM)". In particular, the tensile behaviour was defined through a linear elastic stress-strain relationship with linear softening (see Figure 5). In order to take into account, the age and degradation typically present in masonry bridges, a low tensile strength (f_t) value corresponding to 1/100 of the compressive strength (fc) was considered. In this paper, three types of masonry were considered (M1 solid brick wall and lime mortar , M2 hewn rubble masonry with good texture and M3 rough-hewn rubble masonry as presented in Table 2. In particular, the average values of the specific weight (γ), modulus of elasticity (E) and compressive strength (f_c) obtained from the statistical elaboration of experimental tests reported in Barbieri 2018 [4] were considered in the numerical analysis. The tensile and compressive peak strain (ε_{ty} and ε_{cy}) are respectively equal to f_t/E and f_c/E, compressive ultimate strain (ε_{cu}) is equal to 0.0035 and the tensile fracture energy (G_{ft}) was assumed equal to $0.025(f_c/10)^{0.7}$ as proposed in [63]. It has been supposed that spandrel wall, piers, abutments and archs are made of the same masonry material. The Hauching and backfill have been modelled with a Mohr-Coulomb material considering an friction angle and cohesion equal respectively equal to 20° and 0.05 MPa.

Characteristics		M1	M2	M3
Specific weight	γ [kN/m^3]	18.0	22.0	21.0
Young modulus	E [MPa]	6717	16199	8146
Compressive strength	f_c [MPa]	4.12	4.20	3.87

Table 2 Mechanical characteristics of the masonry

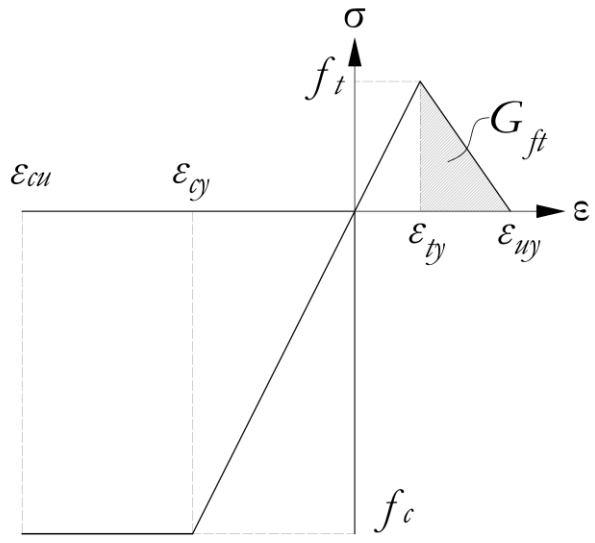

Figure 5 Masonry constitutive law

The commercial software used in this analysis was able to evaluate the crack state at each calculation step. Figure 6 shows the different types of damage possible in relation to the diagram adopted to characterize the tensile behaviour of the masonry.

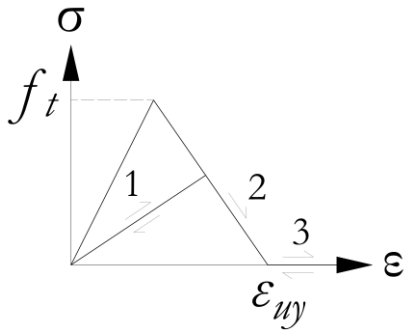

Figure 6 Masonry tensile behaviour: Damage states (1 partially open crack during loading, 2 partially open crack during unloading, 3 fully open crack)

In the study presented in this document, the load reduction applied globally to the structure in the modelling phase is not considered as a pushover analysis. However, the load decrements may occur to individual finite element due to the redistribution of stress caused by the step by step load increment applied to the structure.

As mentioned above, numerical models were used for the modal and pushover analysis of the bridge. With reference to the latter, the thrust profiles proportional to the principal mode in the analysed direction as well as the thrust profiles proportional to the mass of the structure were considered.

The constitutive law model used was able to describe globally the masonry failure phenomena such as crushing and cracking, but was not able to analyse the failure by shear sliding. For each load step of the capacity curve, obtained from the pushover analysis, a shear-sliding verification of the significant sections of the arch and the piers was performed in order to evaluate if the resistant shear (V_{Rd}) was greater than the acting shear (V_{Ed}):

$$V_{Rd} = A_c \cdot (c + f \cdot \sigma_n) \geq V_{Ed} \qquad (1)$$

Where:

A_c is the area of the section in compression;

c is the shear resistance of the masonry in the absence of the normal stress ;

f is the masonry friction coefficient

σ_n is the average compressive stress in the zone of the section (A_c) in compression

In particular, in the pushover curve, only the load values are considered such that the verification given by Eq. 1 is satisfied.

4. Influence of the construction properties on the modal and pushover analysis

4.1. Influence of the haunching, fill, and spandrel walls as resisting elements on the modal and pushover analysis

The results of a preliminary parametric study aiming to analyse how much the "secondary" structural elements of the bridge influence the seismic behaviour of the structure in terms of stiffness, horizontal capacity and modal parameters are reported below.

To this end, 4 models were compared:

- Model 1: the piers, arches and shoulders are structural elements, while the haunching, fill, spandrel walls and ballast are gravitational forces and masses; (Figure 7a).
- Model 2: the piers, the arches, and the shoulders, and the haunching are structural elements while the fill, spandrel walls and ballast are gravitational forces and masses; (Figure 7b).
- Model 3: the piers, the arches, and the shoulders, the haunching and the fill are structural elements while spandrel walls and ballast are gravitational forces and masses; (Figure 7c).
- Model 4: all elements (except the ballast) are considered as structural elements. (Figure 7d).

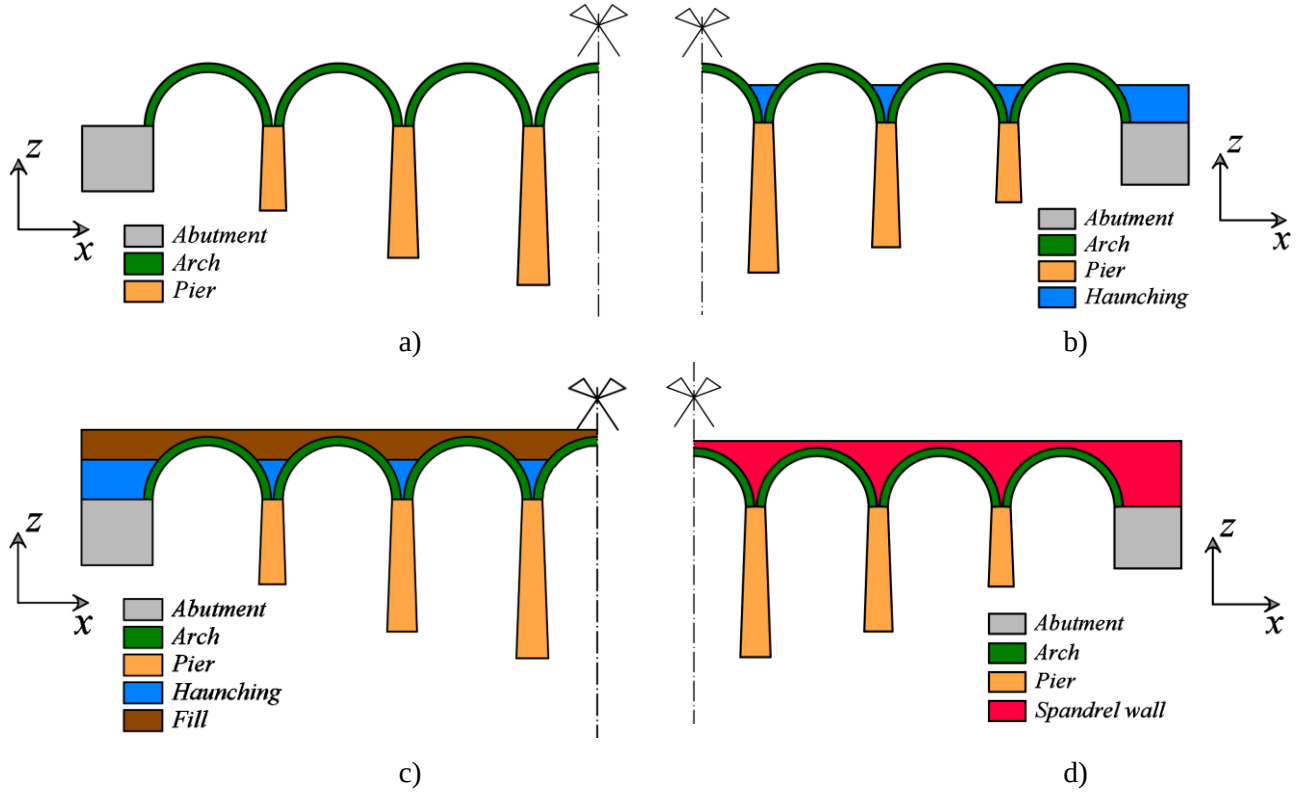

Figure 7 Numerical models investigated. a) Model 1; b) Model 2; c) Model 3; d) Model 4

Initially, a modal analysis was carried out to find out the main vibration mode and the relative modal shapes that excite the bridge masse (M) in the main horizontal directions (X and Y). In particular, from modal analyses, it

emerges that for the four models analysed, the modal shapes (Figure 8) of the fundamental modes in the horizontal directions X and Y are comparable. However, the values of the vibration period (T) and the percentage of excited mass (M_p/M) of the two principal horizontal change according to the different modelling approch, as shown in Table 3. The excited mass $M_{p,j}$ for the j-th mode is equal to:

$$M_{p,j} = \Gamma_j \sum m_i \cdot \Phi_{i,j} \qquad (2)$$

Where:

$\Gamma_j = \frac{\sum m_i \cdot \Phi_{i,j}}{\sum m_i \cdot \Phi_{i,j}^2}$ is the participation factor;

m_i is the mass of the i-th degree of freedom;

$\Phi_{i,j}$ is the i-th component of the j-th vibration mode.

	Model 1		**Model 2**		**Model 3**		**Model 4**	
	1th Mode dir. X	1th Mode dir. Y	1th Mode dir. X	1th Mode dir. Y	1th Mode dir. X	1th Mode dir. Y	1th Mode dir. X	1th Mode dir. Y
T [s]	0.797	0.756	0.559	0.739	0.396	0.753	0.308	0.724
M_p/M [%]	42.33	34.10	50.96	36.32	61.93	37.69	72.33	42.36

Table 3 Modal parameters obtained from the four models analysed.

As can be seen from Table 3, for both directions (X and Y) analysed, but especially for the longitudinal direction (X), the various modelling strategies considered led to big differences in the definition of the vibration period (T) and the percentage of excited mass (M_p/M). In particular, the underestimation of the vibration period of the mode in the longitudinal direction (X) in models 1, and 2 led to a considerable underestimation (compared to the accurate model 4) of the value of the fundamental vibration period that excites the bridge masses in the longitudinal direction (X). This underestimation may cause an incorrect assessment of the seismic action when the non-linear static analysis of the bridge is performed.

In particular, the two frequencies of the principals horizontal modes obtained from the Model 1 are switched respect these obtained from the others three model (Model 2, Model 3 and Model 4). This result has been obtained because the Model 1 better estimate the longitudinal horizontal stiffness of the bridge.

a)

b)

Figure 8 a) first vibration mode in Y) b) first vibration mode in X.

Then, the pushover analyses were carried out for the four models under assessment considering a distribution of proportional horizontal incremental forces in the bridge masses in order to obtain the capacity curves of the bridge in the longitudinal (X) and transverse (Y) directions. The capacity curves (Total base shear - control displacement node) of the multi degrees of freedom system (MDOF) were transformed into capacity curves of a single degree of freedom system (SDOF) and then bilinearised in reference to N2 method [49,50]. The control point considered in the pushover analyses is the centre of the crown section of the central arch.

Table 4 and Table 5 show the points of the bilinearised capacity curves for pushover analyses in X and Y direction respectively. In particular, in these tables the symbol d_i defines one of the two significant values of the displacement in the capacity curve (i=y yield displacement, i=u ultimate displacement) referred to the two pushover analyses in X direction (Table 4) and in Y direction (Table 5). Similarly, with F_i (i=y, u) the reference is made to the yield strength or the ultimate strength for the pushover analysis in the X direction (Table 4) and in the Y direction (Table 5).

	Model 1		Model 2		Model 3		Model 4	
	d_i (m)	F_i (kN)	d_i (m)	F_i (kN)	d_i (m)	F_i (kN)	d_i (m)	F_i (kN)
i = y	0.023	8094.8	0.015	10677.71	0.01	12621.42	0.006	13978.3
i = u	0.049	8094.8	0.026	10677.71	0.023	12621.42	0.049	13978.3

Table 4 Parameters obtained from pushover analysis in X direction.

	Model 1		Model 2		Model 3		Model 4	
	d_i (m)	F_i (kN)	d_i (m)	F_i (kN)	d_i (m)	F_i (kN)	d_i (m)	F_i (kN)
i = y	0.018	7350.8	0.021	8430.255	0.021	8591.059	0.021	9058.037
i = u	0.032	7350.8	0.045	8430.255	0.042	8591.059	0.040	9058.037

Table 5 Parameters obtained from pushover analysis in Y direction.

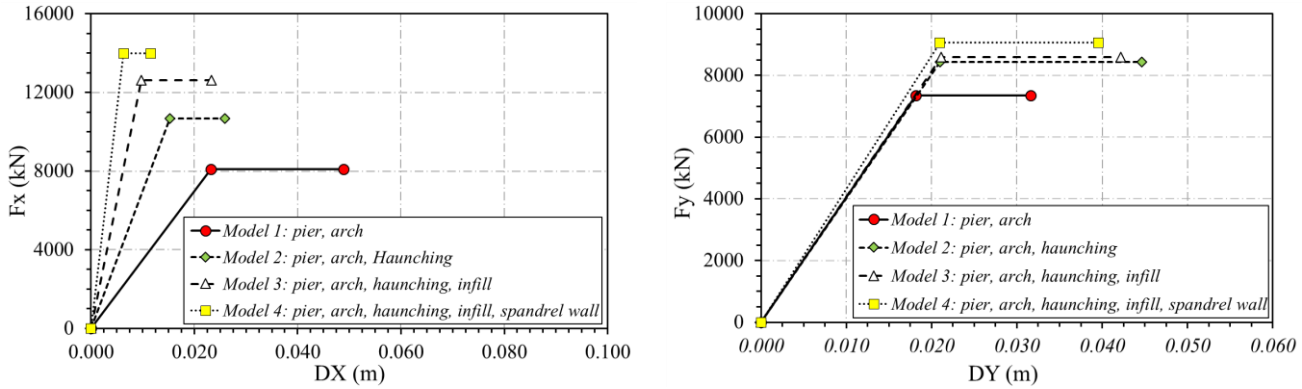

a) *b)*

Figure 9 Pushover analysis. a) X - direction, b) Y - direction

Analysing the bilinear curves of the equivalent SDOF system obtained from the pushover analysis in the X direction (Figure 9a), it can be observed how the stiffness and the ultimate displacement vary drastically as the accuracy of the model under consideration changes, while for the pushover analysis in the Y direction (Figure 9b) this difference is much less evident.

X Direction					Y Direction				
Model	1	2	3	4	Model	1	2	3	4

μ	2.216	2.132	1.970	1.834	μ	2.277	2.129	1.994	1.884
F_y/W	0.091	0.120	0.143	0.158	F_y/W	0.083	0.095	0.097	0.102
M*/M	0.710	0.724	0.728	0.767	M*/M	0.598	0.600	0.632	0.648
K^*/K^*_0	1	2.005	3.724	6.328	K^*/K^*_0	1	0.992	1.003	1.065

Table 6 Equivalent SDOF parameters.

Table 6 also shows the ductility (μ), the normalized stiffness (K^*/K_0^*) of the equivalent SDOF system to that obtained by model 1 (K_0^*), the yield strength (F_y/W) normalized to the weight of the bridge (W) and the mass of the equivalent SDOF system (M^*/M) normalized to the total mass (M):

$$M^* = \Gamma_j \sum m_i \cdot \Phi_{i,j} \qquad (3)$$

By reworking these parameters, the graphs in Figure 10 have been generated, where it can be seen that, for both directions analysed in pushover analysis, models 1, 2 and 3 produce an excessive evaluation of the bridge ductility (Figure 10a) and therefore an overestimation of the real dissipative capacity of the structure. In addition, for the analysis of the longitudinal pushover, neglecting the resisting contribution of the spandrel walls, abutment and fill generally lead to underestimation of the stiffness about 6 times (see Figure 10b). The less refined models (Model 1, Model 2 and Model 3) cautiously define a lower seismic capacity of the bridge, in the longitudinal and transverse direction, than Model 4 (Figure 10c).

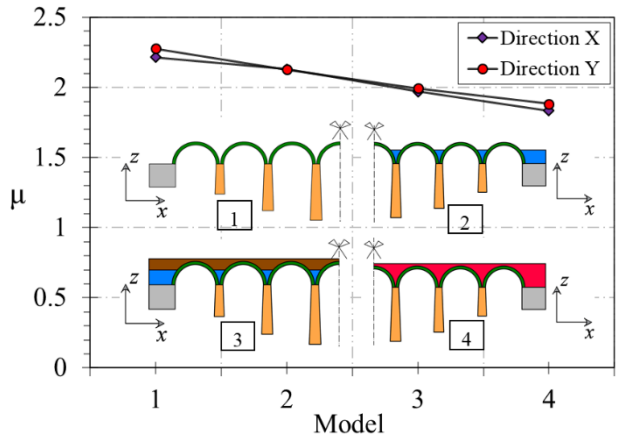

a)

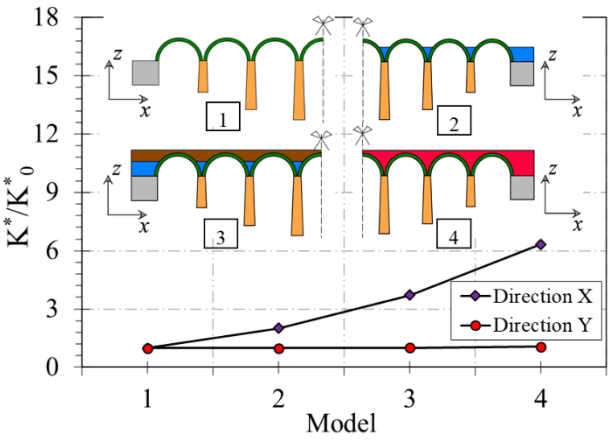

b)

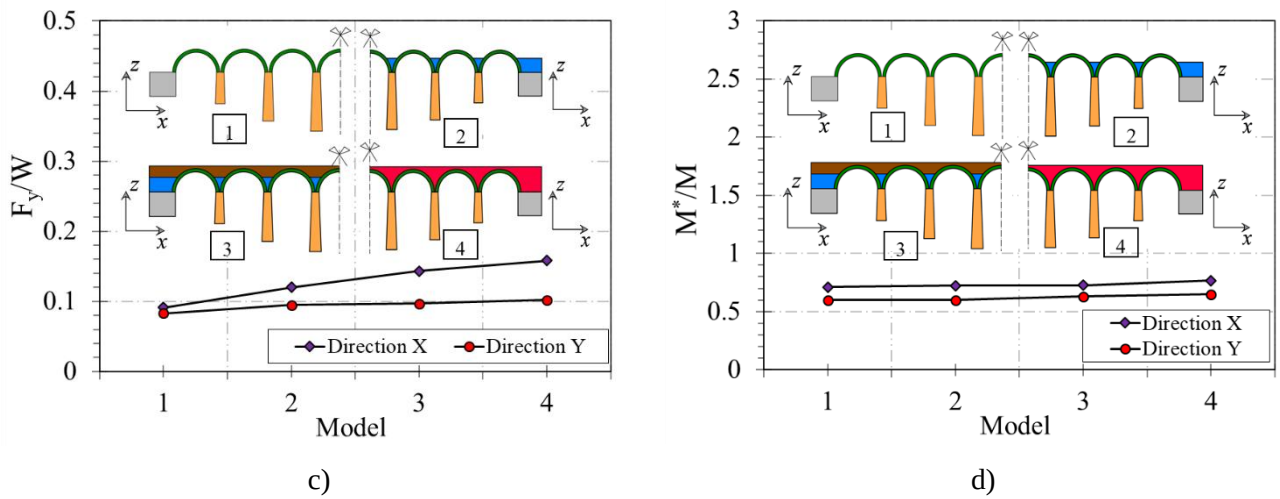

Figure 10 a) ductility; b) stiffness ratio; c) dimensionless yield strength; d) dimensionless mass participation.

4.2. Influence of the haunching and pier properties on the modal and pushover analysis

At this point, the results obtained from a parametric (modal and pushover) analysis are reported and analysed in order to understand the influence of the characteristics of the haunching, the piers cross-section and the type of masonry used to build the masonry bridge under study. The following two geometrical parameters were considered in the parametric analysis:

Normalized height of the haunching (h_r/h_{tot}): As illustrated in the previous section, the presence of the haunching has an effect on the seismic response of the masonry bridge analysed. The influence of the fill height on the overall seismic response of the bridge will be analysed. In particular, three values of h_r/H_{tot} will be considered as shown in Table 1. Specifically, the first value of h_r/H_{tot} is the actual value of the analysed bridge, the third value refers to a haunching that reaches the extrados in the keystone section of the arch and the second value is an intermediate value between the first and the third.

Normalized external thickness of the pier (D^*/D): sometimes, the cross-section of the masonry bridge piers is characterised by an outer layer of masonry with good mechanical characteristics and an inner core made of fill material with worse mechanical characteristics. In the parametric analysis four values of the parameter D^*/D (Table 1) were considered to analyse the effects of the hollow cross-section of the piers in the seismic response and the definition of the bridge collapse mode under ultimate conditions.

The parametric analysis has been developed considering the three types of masonry shown in Table 2. In particular, Figures 11, 12, 13 show the synthetic results obtained from pushover analysis in the X direction considering the M1, M2 and M3 masonry types. Similarly, Figures 14, 15, 16 show the summary results of pushover analysis in the Y direction considering the type of masonry M1, M2 and M3.

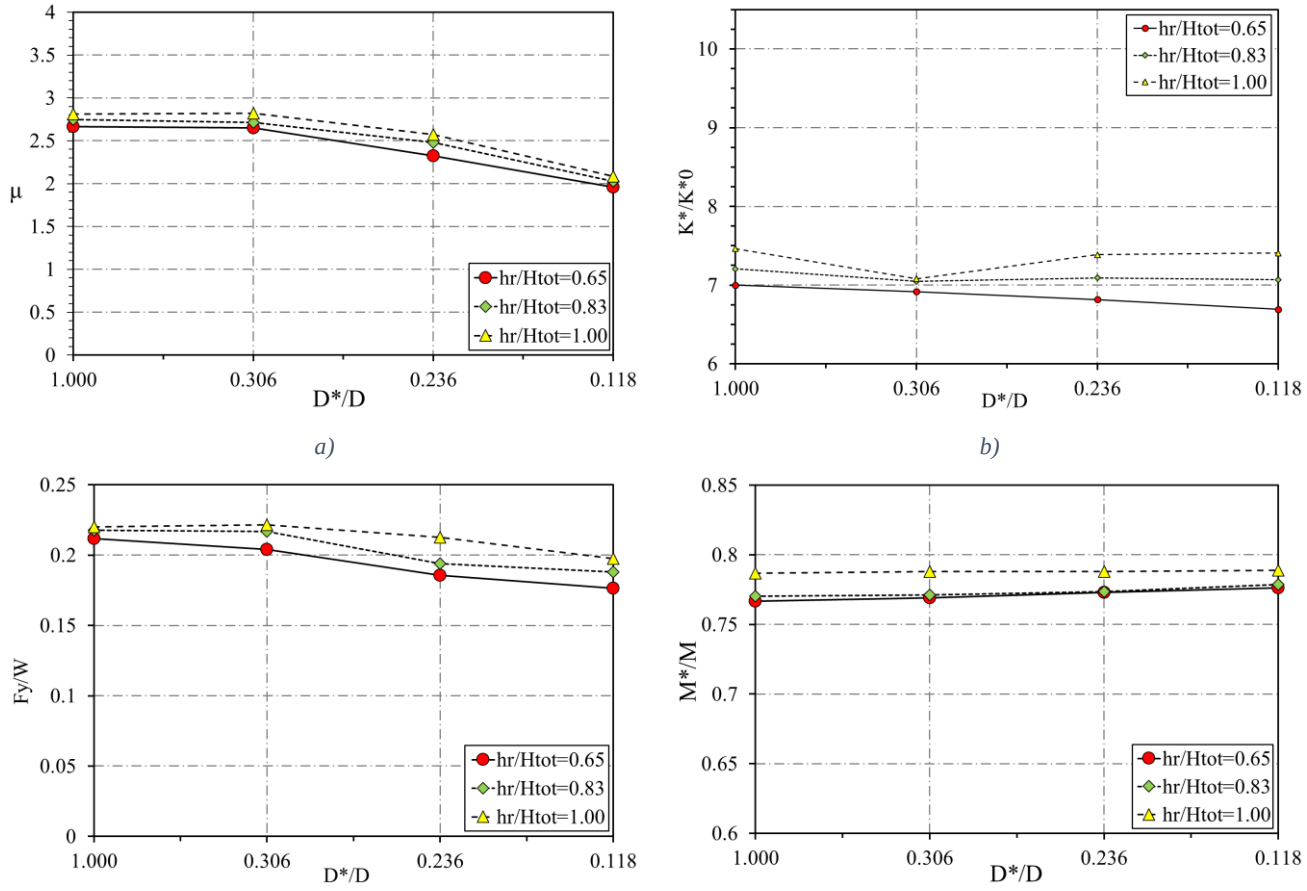

a) *b)* *c)* *d)*

Figure 11 Masonry typology M1. a) Ductility; b) stiffness ratio, c) Normalized yielding force; d) Normalized mass participation. (X direction)

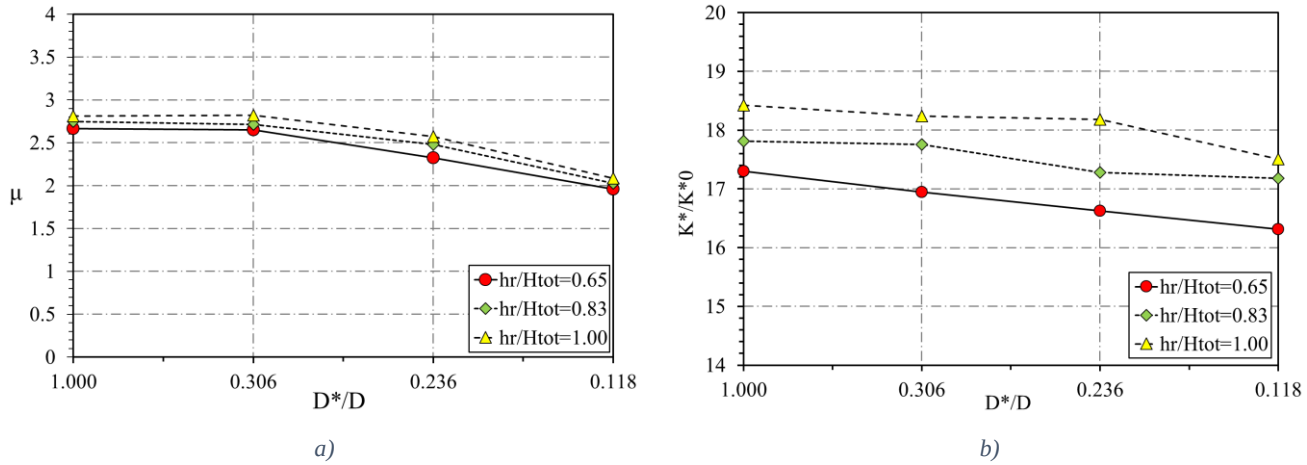

a) *b)*

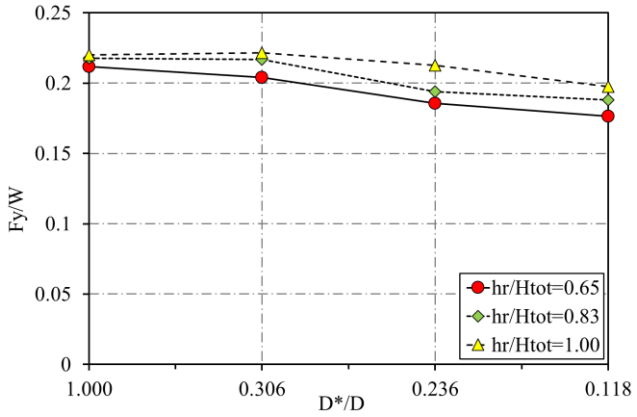

c)

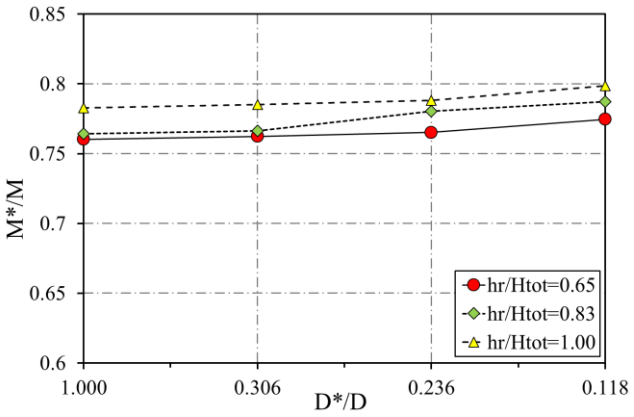

d)

Figure 12 Masonry Typology M2. a) ductility; b) stiffness ratio, c) Normalized yielding force; d) Normalized mass participation. (X direction)

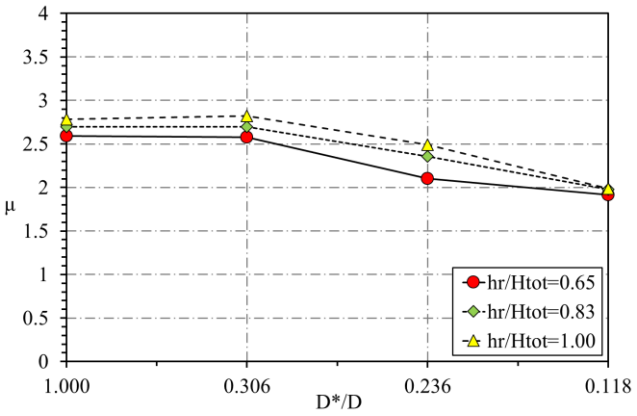

a)

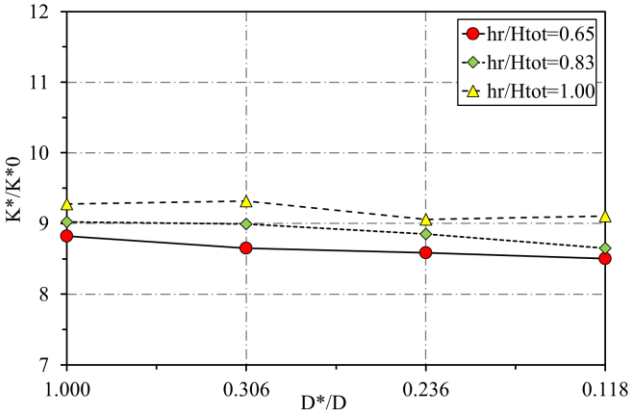

b)

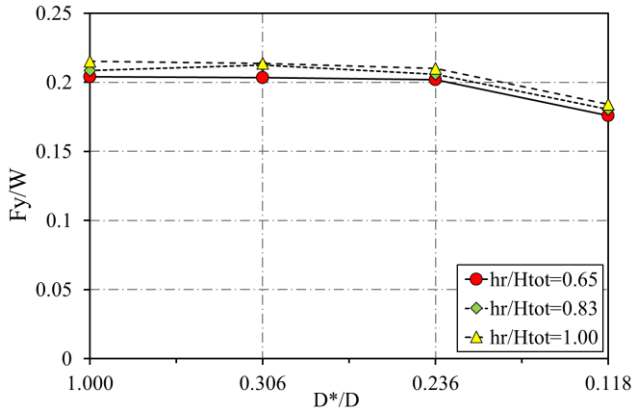

c)

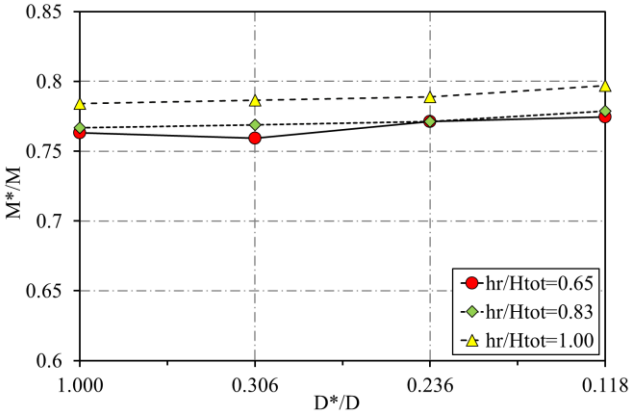

d)

Figure 13 Masonry Typology M3. a) ductility; b) stiffness ratio, c) Normalized yielding force; d) Normalized mass participation. (X direction)

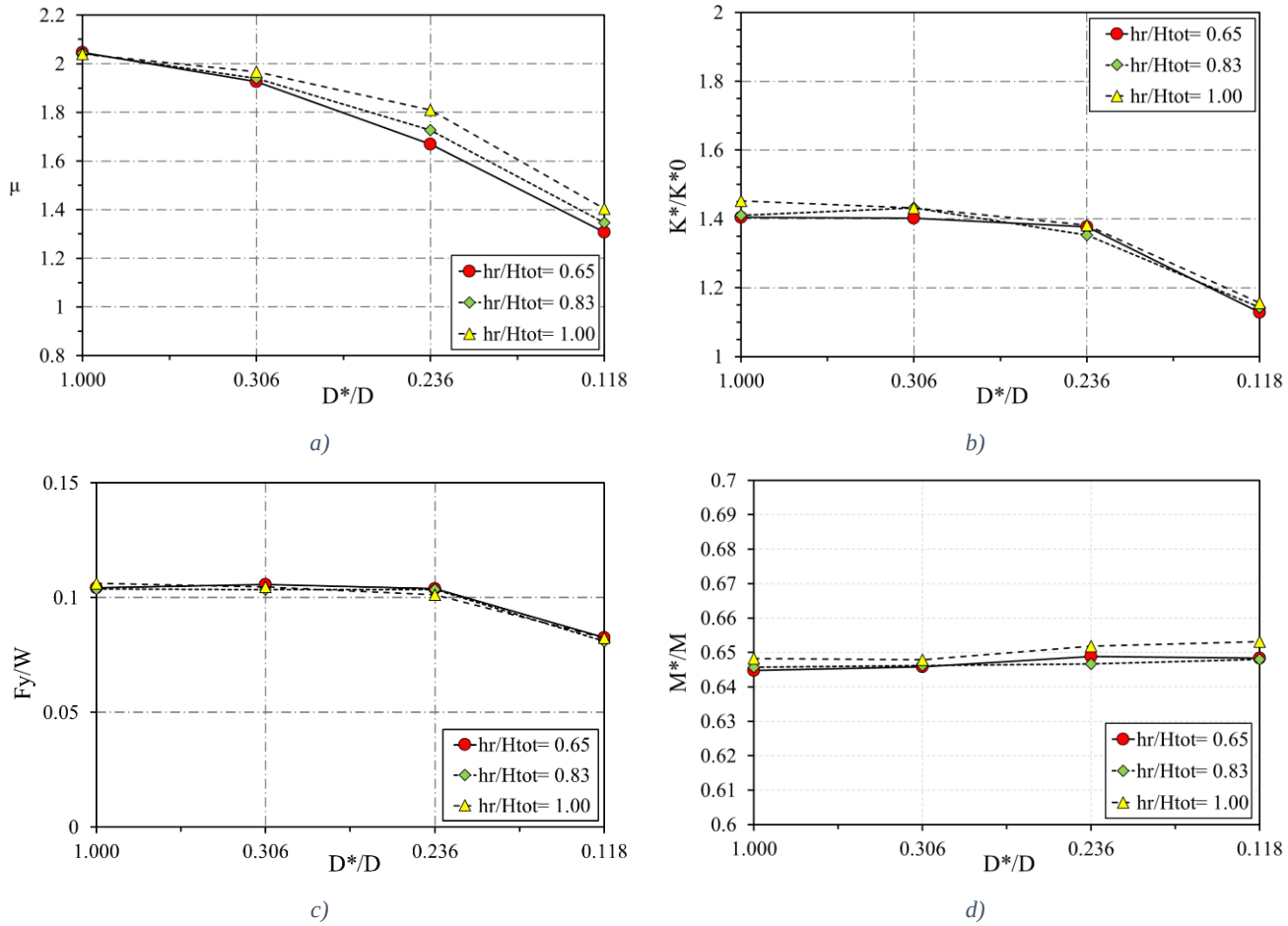

Figure 14 Masonry typology M1. a) ductility; b) stiffness ratio, c) Normalized yielding force; d) Normalized mass participation. (Y direction)

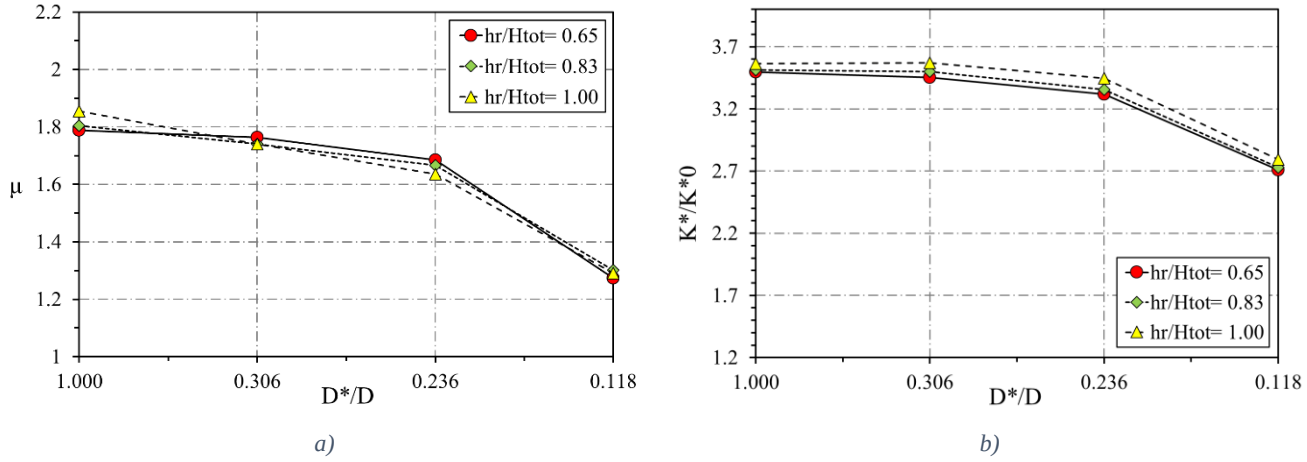

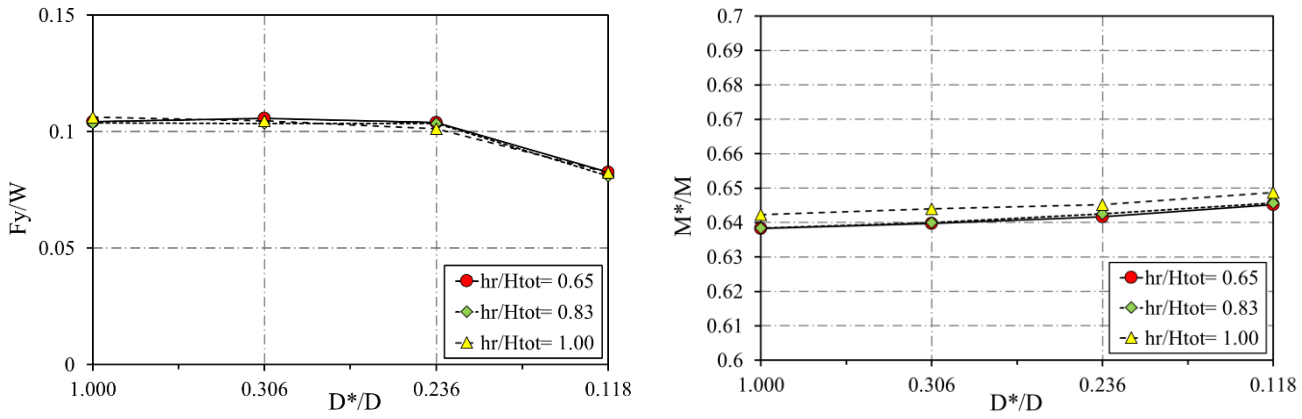

c) *d)*

Figure 15 Masonry Typology M2. a) ductility; b) stiffness ratio, c) Normalized yielding force; d) Normalized mass participation.

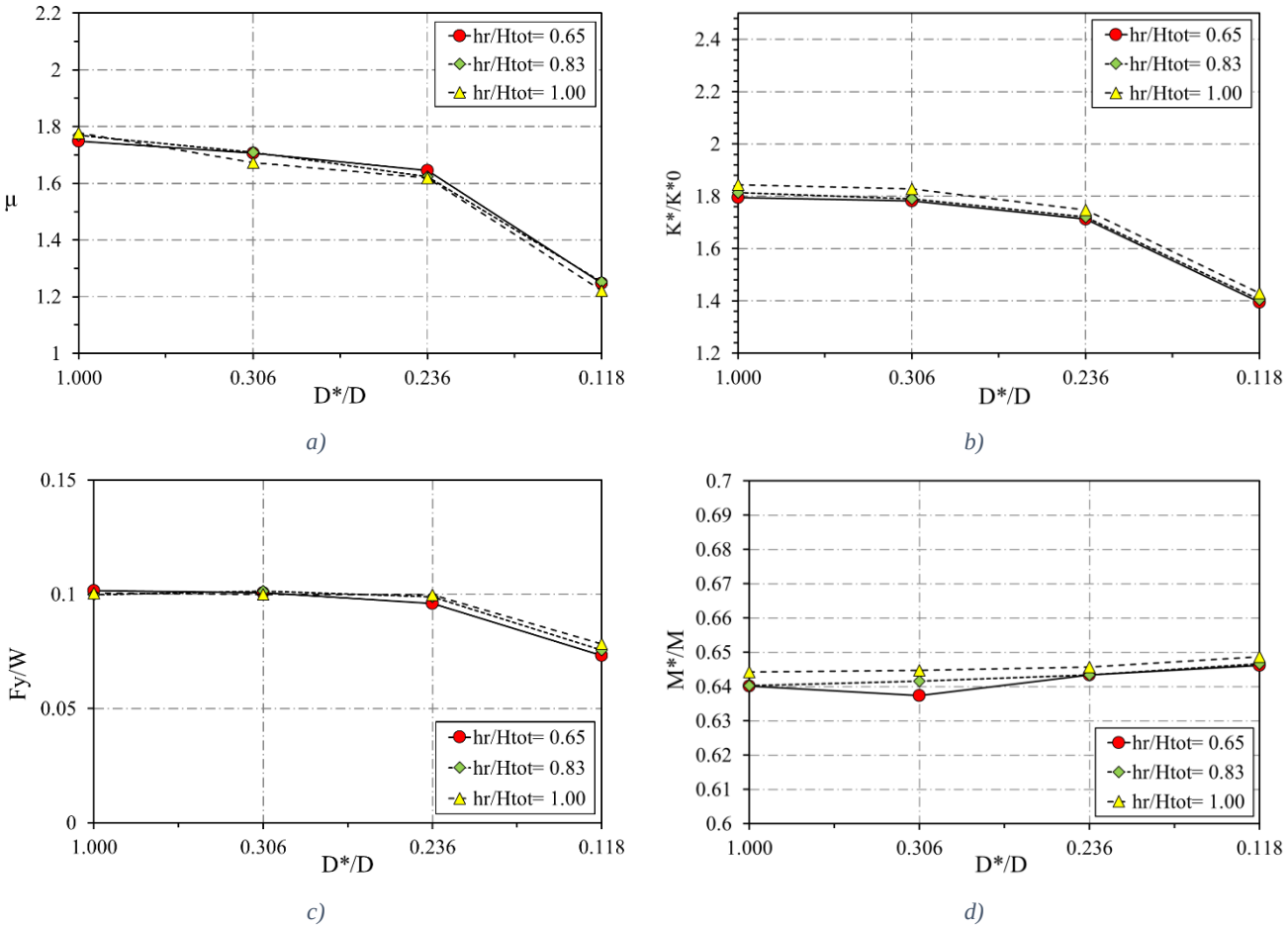

a) *b)*

c) *d)*

Figure 16 Masonry Typology M3. a) ductility; b) stiffness ratio, c) Normalized yielding force; d) Normalized mass participation.

The first analysis of the graphs in Figures 11, 12, 13, 14, 15 and 16 shows that the h_r/H_{tot} parameter and the different types of masonry have a little influence on the seismic response of the bridge analysed with respect to the D^*/D parameter.

From Figures 11a, 12a, 13a, 14a, 15a and 16a it can be seen that for the pushover analysis in both the longitudinal and transversal directions, the ductility decreases as the D^*/D ratio decreases because, as will be explained later, the piers with a small outer layer tend to develop a fragile mechanism in the seismic conditions. Similarly, the normalized stiffness K^*/K^*_0 and capacity f_y/W also decrease as the area of the loose material in the cross-section of the pier increases. However, it should be noted that the f_y/W seismic capacity is reduced when the thickness of the outer pier layer is modest ($D^*/D<0.236$) compared to the total pier thickness (see Figures 11c, 12c, 13c, 14c, 15c and 16c). Finally, it can be observed (see Figures 11d, 12d, 13d, 14d, 15d and 16d) that the mass of the equivalent SDOF system is slightly affected by the D^*/D parameter.

5. Discussion of the results

In the previous sections, it has been found that the haunching, the fill, the spandrel walls and the cross-section of the pier have an influence on the overall seismic response of the bridge. This section analyses the contribution of these parameters in defining the global mechanisms of bridge collapse in the ultimate seismic conditions.

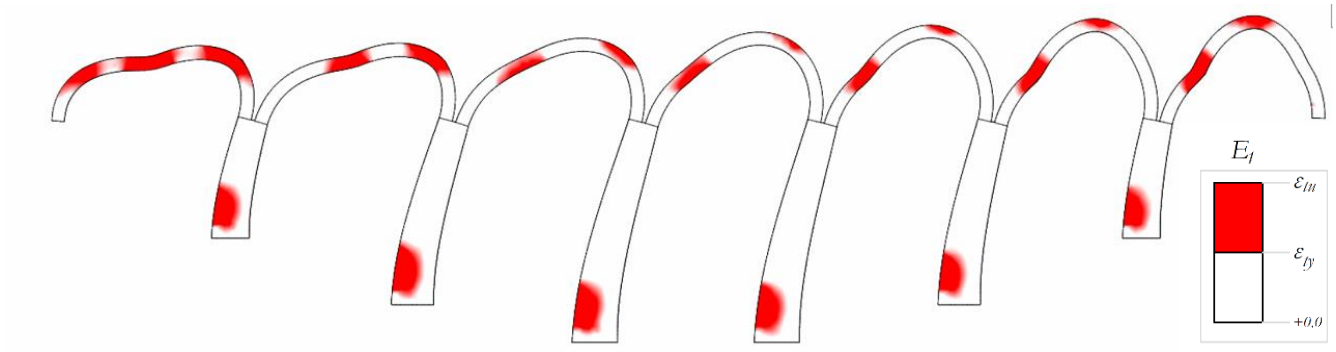

Figure 17 Model 1, pushover analysis in X, crack contour in the longitudinal section of the bridge.

By analysing the longitudinal behaviour of the bridge, it can be observed that multi-arch masonry structures (Figure 17) typically develop collapse mechanisms characterized by the formation of hinges at the base of the piers and two hinges located in the arches (Figure 17). In masonry arch bridges, the presence of haunching, fill and spandrel walls contrasts with the formation of hinges in the arch, as can be seen from the cracked contour zones obtained from model 4 and shown in Figure 18. For these reasons, the haunching, fill and spandrel walls contribute to the seismic capacity of the bridge. Moreover, the collapse mechanism of the masonry bridge (Figure 18), considering all the resisting elements of the bridge, is less ductile than that shown in Figure 17.

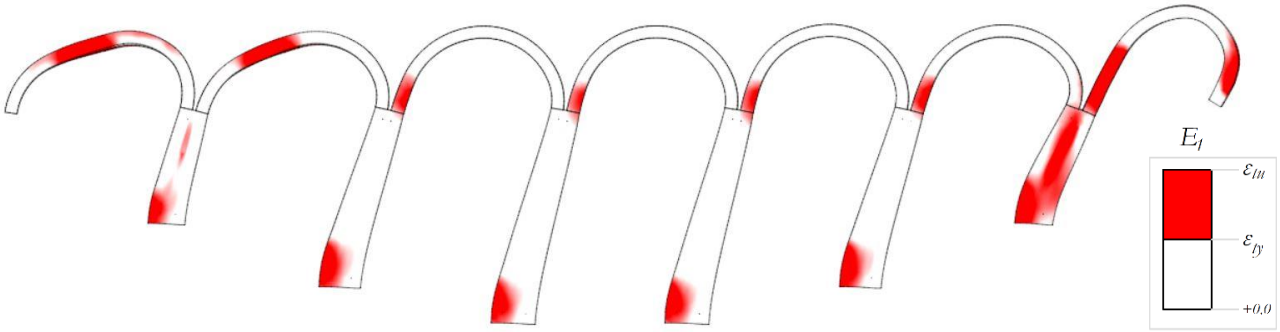

Figure 18 Model 4, pushover analysis in X, crack contour in the longitudinal section of the bridge.

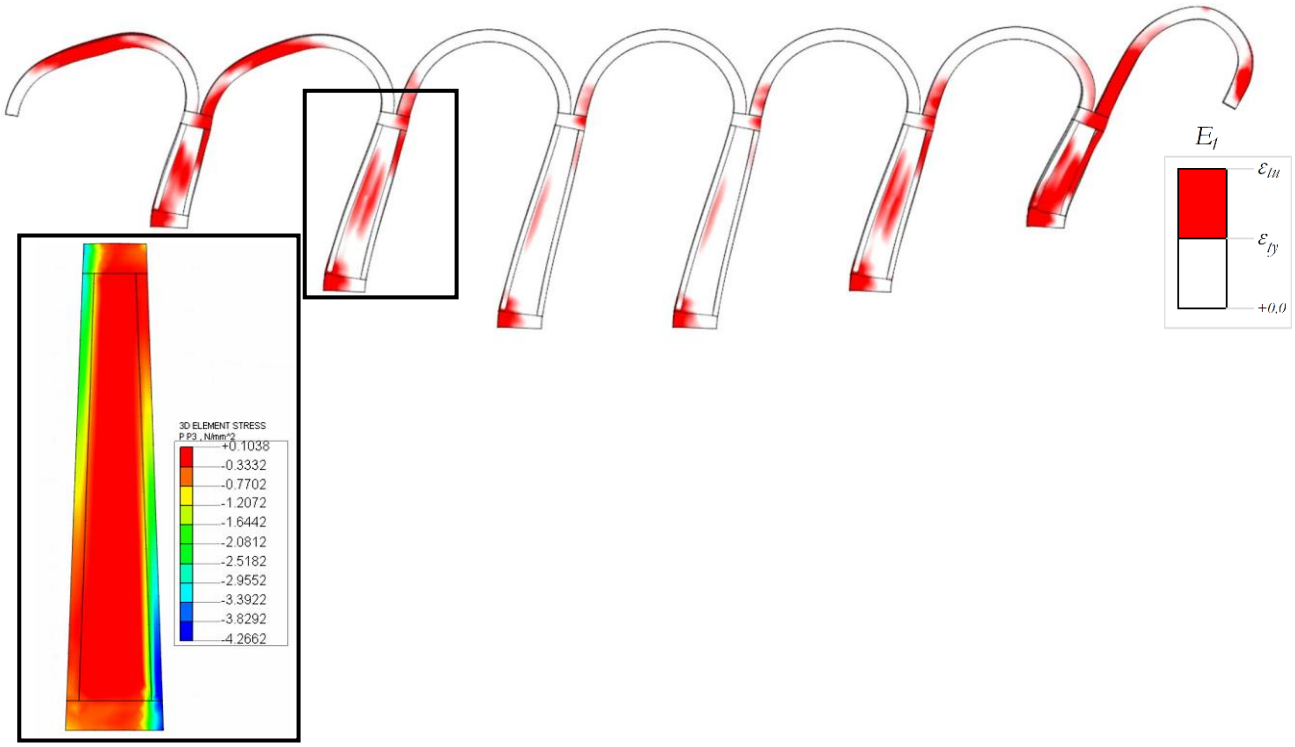

Figure 19 Model with D/D=0.118, pushover analysis in X, crack contour in the longitudinal section of the bridge.*

An interesting aspect to underline is the different mode of failure between the full piers (Figure 18) and the hollow piers with a modest external thickness compared to the whole section (Figure 19). In fact, the presence of an internal core made of poor mechanical properties material causes (in ultimate conditions) the decoupling between the external and internal part of the pier (Figure 19). In addition, the stress states of compression concentrated in the external area of the pier are created with possible development of localised buckling phenomena.

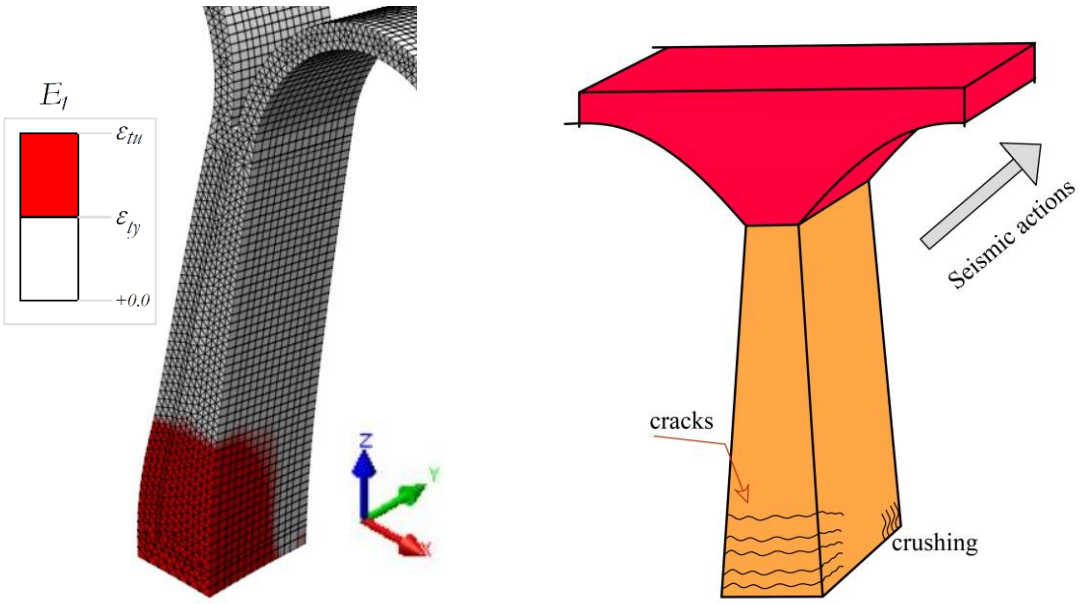

Figure 20 a) Model with D/D=1, pushover analysis in Y, crack contour in the longitudinal section of the bridge. b) collapse mechanism of the pier*

The analyses have shown that hollow piers also influence the mode of collapse considered to be a seismic action across the bridge. In particular, if the section of the pier is full, because the pier is slender, a failure to the combined bending at the base section develops under ultimate conditions (Figure 20).

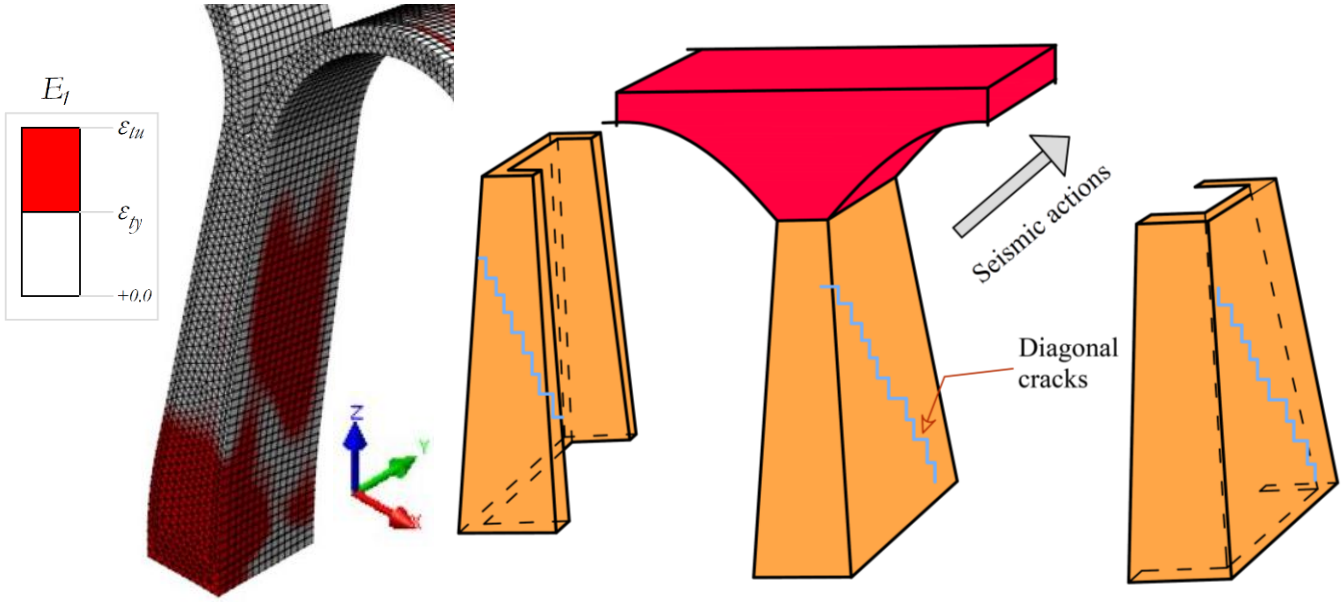

Figure 21 Model with D/D=0.118, pushover analysis in Y, crack contour in the longitudinal section of the bridge. b) Collapse mechanism of the pier*

Figure 22 Claro River Bridge: diagonal cracks in a bridge pier [59].

On the other hand, if the pier is hollow (Figure 21), the collapse mechanism of the pier is different. In particular, near the base section, the pier will be subjected to cracking in the area where normal tensile stresses develop; in addition, diagonal cracks have been observed in the outer walls of the pier (Figure 21a). Then, there has been a diagonal shear failure of the outer walls of the piers which are being subjected to in-plane seismic action (Figure 21b). The same damage and crack initiation and propagation were observed in the pier of the Claro River Bridges (Figure 22) after the earthquake.

6. Conclusion

This work highlights some important aspects of the seismic behaviour of multi-span slender masonry arch bridges. These kind of bridges are classified as the most vulnerable category of masonry bridge to seismic action compared to other types of masonry bridges. Therefore, in regions of high seismic hazards, they need to be monitored and their vulnerability to seismic action assessed. As this study has shown, it is of fundamental importance to take into account in the seismic verification of masonry bridges:

- The actual strength and rigidity of the haunching, fill and spandrel walls. In fact, considering these elements as weights on the structure can lead to an overestimation of the ductility and fundamental periods of the structure and an underestimation of the rigidity and capacity of the structure. A poor definition of these parameters, which come into play in seismic verification by non-linear static analysis, may produce an incorrect estimate of the actual vulnerability of the bridge. In addition, considering in seismic analysis the haunching, fill and tympanums exclusively as weights could (in some cases) also lead to underestimation of the actual vulnerability of the structure.

- The actual cross-section configuration of the piers, perhaps through the use of on-site tests that define in detail their thicknesses and constituent materials. In fact, piers with a modest external thickness of good characteristics and an internal core made of filling material are more vulnerable to transverse and longitudinal seismic action than piers with a solid section made of good masonry. In particular, for hollow piers, the collapse mechanisms of the element that develop due to less seismic action change compared to those that activate the combined bending failure that develops in the case of piers with solid section. In particular, if we analyse the longitudinal behaviour of the bridge, the collapse of the pier occurs by centred compression of the external area of the section, while in the case of transversal seismic action a diagonal shear failure of the side walls of the piers develops. This situation brings different results in terms of the resistance and ductility of the hollow pier with respect to the solid section pier.

References

[1] Melbourne C, Wang J, Tomor AK. A new masonry arch bridge assessment strategy (SMART). Proc Inst Civ Eng Bridg Eng 2007;160:81–7. doi:10.1680/bren.2007.160.2.81.

[2] Brencich A, Sabia D. Experimental identification of a multi-span masonry bridge: The Tanaro Bridge. Constr Build Mater 2008;22:2087–99. doi:10.1016/j.conbuildmat.2007.07.031.

[3] Zanini MA, Hofer L, Faleschini F, Zampieri P, Fabris N, Pellegrino C. Preliminary macroseismic survey of the 2016 amatrice seismic sequence. Ann Geophys 2016;59. doi:10.4401/ag-7172.

[4] Barbieri DM. Two methodological approaches to assess the seismic vulnerability of masonry bridges. J Traffic Transp Eng (English Ed 2019;6:49–64. doi:10.1016/j.jtte.2018.09.003.

[5] Cavalagli N, Kita A, Castaldo VL, Pisello AL, Ubertini F. Hierarchical environmental risk mapping of material degradation in historic masonry buildings: An integrated approach considering climate change and structural damage. Constr Build Mater 2019;215:998–1014. doi:10.1016/j.conbuildmat.2019.04.204.

[6] Milani G, Lourenço PB. 3D non-linear behavior of masonry arch bridges. Comput Struct 2012;110–111:133–50. doi:10.1016/j.compstruc.2012.07.008.

[7] Melbourne C, Gilbert M. Behaviour of multiring brickwork arch bridges. Struct Eng London 1995;73:39–47.

[8] Baraldi D, Reccia E, Cecchi A. In plane loaded masonry walls: DEM and FEM/DEM models. A critical review. Meccanica 2018;53:1613–28. doi:10.1007/s11012-017-0704-3.

[9] Portioli FPA. Rigid block modelling of historic masonry structures using mathematical programming: a unified formulation for non-linear time history, static pushover and limit equilibrium analysis. Bull Earthq Eng 2019;18:211–39. doi:10.1007/s10518-019-00722-0.

[10] Sarhosis V, Forgács T, Lemos J V. A discrete approach for modelling backfill material in masonry arch

bridges. Comput Struct 2019;224:106108. doi:10.1016/j.compstruc.2019.106108.

[11] Cannizzaro F, Pantò B, Caddemi S, Caliò I. A Discrete Macro-Element Method (DMEM) for the nonlinear structural assessment of masonry arches. Eng Struct 2018;168:243–56. doi:10.1016/j.engstruct.2018.04.006.

[12] Zampieri P, Perboni S, Tetougueni CD, Pellegrino C. Different Approaches to Assess the Seismic Capacity of Masonry Bridges by Non-linear Static Analysis 2020;6. doi:10.3389/fbuil.2020.00047.

[13] Sarhosis V, De Santis S, de Felice G. A review of experimental investigations and assessment methods for masonry arch bridges. Struct Infrastruct Eng 2016;12:1439–64. doi:10.1080/15732479.2015.1136655.

[14] Cecchi A, Milani G. A kinematic FE limit analysis model for thick English bond masonry walls. Int J Solids Struct 2008;45:1302–31. doi:10.1016/j.ijsolstr.2007.09.019.

[15] Melbourne C, Gilbert M, Wagstaff M. The collapse behaviour of multispan brickwork arch bridges. Struct Eng 1997;75:297–305.

[16] Zhang Y, Tubaldi E, Macorini L, Izzuddin BA. Mesoscale partitioned modelling of masonry bridges allowing for arch-backfill interaction. Constr Build Mater 2018;173:820–42. doi:10.1016/j.conbuildmat.2018.03.272.

[17] Tubaldi E, Macorini L, Izzuddin BA. Three-dimensional mesoscale modelling of multi-span masonry arch bridges subjected to scour. Eng Struct 2018;165:486–500. doi:10.1016/j.engstruct.2018.03.031.

[18] Zhang Y, Macorini L, Izzuddin BA. Numerical investigation of arches in brick-masonry bridges. Struct Infrastruct Eng 2018;14:14–32. doi:10.1080/15732479.2017.1324883.

[19] Tubaldi E, Macorini L, Izzuddin BA. Identification of critical mechanical parameters for advanced analysis of masonry arch bridges. Struct Infrastruct Eng 2019;0:1–18. doi:10.1080/15732479.2019.1655071.

[20] Bertolesi E., Milani G., Lopane F., Acito M. (2017). Augustus Bridge in Narni (Italy): Seismic vulnerability assessment of the still standing part, possible causes of collapse and importance of the Roman concrete infill in the seismic-resistant behavior. International Journal of Architectural Heritage. 11(5), pp. 717-746. DOI: 10.1080/15583058.2017.1300712

[21] Reccia, E., Milani, G., Cecchi, A., Tralli, A. Full 3D homogenization approach to investigate the behavior of masonry arch bridges: The Venice trans-lagoon railway bridge (2014) Construction and Building Materials, 66, pp. 567-586. DOI: 10.1016/j.conbuildmat.2014.05.096

[22] Forgács T, Sarhosis V, Bagi K. Influence of construction method on the load bearing capacity of skew masonry arches. Eng Struct 2018;168:612–27. doi:10.1016/j.engstruct.2018.05.005.

[23] D'Altri AM, Sarhosis V, Milani G, Rots J, Cattari S, Lagomarsino S, et al. Modeling Strategies for the Computational Analysis of Unreinforced Masonry Structures: Review and Classification. Springer Netherlands; 2019. doi:10.1007/s11831-019-09351-x.

[24] Forgács T, Sarhosis V, Bagi K. Minimum thickness of semi-circular skewed masonry arches. Eng Struct 2017;140:317–36. doi:10.1016/j.engstruct.2017.02.036.

[25] Cavalagli N, Gusella V, Severini L. The safety of masonry arches with uncertain geometry. Comput Struct 2017;188:17–31. doi:10.1016/j.compstruc.2017.04.003.

[26] Zampieri P, Cavalagli N, Gusella V, Pellegrino C. Collapse displacements of masonry arch with geometrical uncertainties on spreading supports. Comput Struct 2018;208:118–29. doi:10.1016/j.compstruc.2018.07.001.

[27] Cavalagli N, Gusella V, Severini L. Lateral loads carrying capacity and minimum thickness of circular and pointed masonry arches. Int J Mech Sci 2016;115–116:645–56. doi:10.1016/j.ijmecsci.2016.07.015.

[28] Galassi S, Ruggieri N, Tempesta G. A Novel Numerical Tool for Seismic Vulnerability Analysis of Ruins in Archaeological Sites. Int J Archit Herit 2018;00:1–22. doi:10.1080/15583058.2018.1492647.

[29] Galassi S, Misseri G, Rovero L, Tempesta G. Failure modes prediction of masonry voussoir arches on moving supports. Eng Struct 2018;173:706–17. doi:10.1016/j.engstruct.2018.07.015.

[30] Galassi S. A numerical procedure for failure mode detection of masonry arches reinforced with fiber reinforced polymeric materials. IOP Conf Ser Mater Sci Eng 2018;369. doi:10.1088/1757-899X/369/1/012038.

[31] Milani G., Tralli A. (2011). Simple SQP approach for out-of-plane loaded homogenized brickwork panels accounting for softening. Computers & Structures, 89(1-2), pp. 201-215.doi:10.1016/j.compstruc.2010.09.005.

[32] Gilbert M, Casapulla C, Ahmed HM. Limit analysis of masonry block structures with non-associative frictional joints using linear programming. Comput Struct 2006;84:873–87. doi:10.1016/j.compstruc.2006.02.005.

[33] Cascini L, Gagliardo R, Portioli F. LiABlock_3D: A Software Tool for Collapse Mechanism Analysis of Historic Masonry Structures. Int J Archit Herit 2018;14:75–94. doi:10.1080/15583058.2018.1509155.

[34] Pantò B, Cannizzaro F, Caddemi S, Caliò I, Chácara C, Lourenço PB. Nonlinear modelling of curved masonry structures after seismic retrofit through FRP reinforcing. Buildings 2017;7:1–17. doi:10.3390/buildings7030079.

[35] Caliò I, Marletta M, Pantò B. A new discrete element model for the evaluation of the seismic behaviour of unreinforced masonry buildings. Eng Struct 2012;40:327–38. doi:10.1016/j.engstruct.2012.02.039.

[36] Caliò I, Pantò B. A macro-element modelling approach of Infilled Frame Structures. Comput Struct 2014;143:91–107. doi:10.1016/j.compstruc.2014.07.008.

[37] D'Altri A.M., de Miranda S., Milani G., Castellazzi G. (2020). A numerical procedure for the force-displacement description of out-of-plane collapse mechanisms in masonry structures. Computers & Structures, 233. https://doi.org/10.1016/j.compstruc.2020.106234

[38] Zampieri, P., Amoroso, M., Pellegrino, C. The masonry buttressed arch on spreading support(2019) Structures, 20, pp. 226-236. DOI: 10.1016/j.istruc.2019.03.008

[39] Zampieri, P., Simoncello, N., Pellegrino, C. Structural behaviour of masonry arch with no-horizontal springing settlement (2018) Frattura ed Integrita Strutturale, 12 (43), pp. 182-190. DOI: 10.3221/IGF-ESIS.43.14

[40] Zampieri, P., Faleschini, F., Zanini, M.A., Simoncello, N. Collapse mechanisms of masonry arches with settled springing(2018) Engineering Structures, 156, pp. 363-374. DOI: 10.1016/j.engstruct.2017.11.048.

[41] Simoncello, N., Zampieri, P., Gonzalez-Libreros, J., Pellegrino, C. Experimental behaviour of damaged masonry arches strengthened with steel fiber reinforced mortar (SFRM)(2019) Composites Part B: Engineering, 177 DOI: 10.1016/j.compositesb.2019.107386

[42] Di Carlo F, Coccia S, Rinaldi Z. Collapse load of a masonry arch after actual displacements of the supports. Arch Appl Mech 2018;88:1545–58. doi:10.1007/s00419-018-1386-6.

[43] Tiberti S, Grillanda N, Mallardo V, Milani G. A Genetic Algorithm adaptive homogeneous approach for evaluating settlement-induced cracks in masonry walls. Eng Struct 2020;221:111073. doi:10.1016/j.engstruct.2020.111073.

[44] Tralli A, Chiozzi A, Grillanda N, Milani G. International Journal of Solids and Structures Masonry structures in the presence of foundation settlements and unilateral contact problems 2020;192:187–201. doi:10.1016/j.ijsolstr.2019.12.005.

[45] Scozzese F, Ragni L, Tubaldi E, Gara F. Modal properties variation and collapse assessment of masonry arch bridges under scour action. Eng Struct 2019;199:109665. doi:10.1016/j.engstruct.2019.109665.

[46] Zampieri P, Zanini MA, Faleschini F, Hofer L, Pellegrino C. Failure analysis of masonry arch bridges subject to local pier scour. Eng Fail Anal 2017;79. doi:10.1016/j.engfailanal.2017.05.028.

[47] Marefat MS, Yazdani M, Jafari M. Seismic assessment of small to medium spans plain concrete arch bridges. Eur J Environ Civ Eng 2019;23:894–915. doi:10.1080/19648189.2017.1320589.

[48] Mahmoudi Moazam A, Hasani N, Yazdani M. Incremental dynamic analysis of small to medium spans plain concrete arch bridges. Eng Fail Anal 2018;91:12–27. doi:10.1016/j.engfailanal.2018.04.027.

[49] Homaei F, Yazdani M. The probabilistic seismic assessment of aged concrete arch bridges: The role of soil-structure interaction. Structures. 2020;28:894-904.

[50] Jahangiri V, Yazdani M. Seismic reliability and limit state risk evaluation of plain concrete arch bridges. Structure and Infrastructure Engineering. 2021;17:170-90.

[51] De Santis S, de Felice G. A fibre beam-based approach for the evaluation of the seismic capacity of masonry arches Stefano. Earthq Eng Struct Dyn 2014:1–6. doi:10.1002/eqe.

[52] Zampieri P, Tecchio G, da Porto F, Modena C. Limit analysis of transverse seismic capacity of multi-span masonry arch bridges. Bull Earthq Eng 2015;13. doi:10.1007/s10518-014-9664-3.

[53] Zampieri P, Zanini MA, Faleschini F. Derivation of analytical seismic fragility functions for common masonry bridge types: methodology and application to real cases. Eng Fail Anal 2016;68. doi:10.1016/j.engfailanal.2016.05.031.

[54] da Porto F, Tecchio G, Zampieri P, Modena C, Prota A. Simplified seismic assessment of railway masonry arch bridges by limit analysis. Struct Infrastruct Eng 2016;12. doi:10.1080/15732479.2015.1031141.

[55] Zampieri P. Horizontal capacity of single-span masonry bridges with intrados FRCM strengthening. Compos Struct 2020;244:112238. doi:10.1016/j.compstruct.2020.112238.

[56] Zampieri P, Simoncello N, Pellegrino C. Seismic capacity of masonry arches with irregular abutments and arch thickness. Constr Build Mater 2019;201:786–806. doi:10.1016/j.conbuildmat.2018.12.063.

[57] Zampieri P, Zanini MA, Modena C. Simplified seismic assessment of multi-span masonry arch bridges. Bull Earthq Eng 2015;13. doi:10.1007/s10518-015-9733-2.

[58] Mohsen Rahnama. The 2010 Maule, Chile Earthquake: Lessons and Future Challenges 2010.

[59] Gaetani A, Lourenço PB, Monti G, Moroni M. Shaking table tests and numerical analyses on a scaled dry-joint arch undergoing windowed sine pulses. Bull Earthq 2017;15:4939–61.

[60] Fanning PJ, Boothby TE. Three-dimensional modelling and full-scale testing of stone arch bridges. Comput Struct 2001;79:2645–62. https://doi.org/10.1016/ S0045-7949(01)00109-2.

[61] Aytulun E, Soyoz S, Karcioglu E. System Identification and Seismic Performance Assessment of a Stone Arch Bridge. J Earthq Eng 2019:1–21. https://doi.org/ 10.1080/13632469.2019.1692740.

[62] Boothby T, Yurianto Y, Erdogmus E. Experimental replication of masonry arch bridge spandrel wall collapse. TMS J 2005:37–46.

[63] Ghiassi, B., Vermelfoort, A.T., Lourenço, P.B. Masonry mechanical properties (2019) Numerical Modeling of Masonry and Historical Structures: From Theory to Application, pp. 239-261. DOI: 10.1016/B978-0-08-102439-3.00007-5

[62] Fajfar, P. Capacity spectrum method based on inelastic demand spectra (1999) Earthquake Engineering and Structural Dynamics, 28 (9), pp. 979-993. DOI: 10.1002/(SICI)1096-9845(199909)28:9<979::AID-EQE850>3.0.CO;2-1

[63] F Fajfar, P., Gašperšič, P. The N2 method for the seismic damage analysis of RC buildings (1996) Earthquake Engineering and Structural Dynamics, 25 (1), pp. 31-46. DOI: 10.1002/(SICI)1096-9845(199601)25:1<31::AID-EQE534>3.0.CO;2-V